

# InstantGroup: Instant Template Generation for Scalable Group of Brain MRI Registration

Ziyi He and Albert C. S. Chung

**Abstract**—Template generation is a critical step in groupwise image registration, which involves aligning a group of subjects into a common space. While existing methods can generate high-quality template images, they often incur substantial time costs or are limited by fixed group scales. In this paper, we present InstantGroup, an efficient groupwise template generation framework based on variational autoencoder (VAE) models that leverage latent representations’ arithmetic properties, enabling scalability to groups of any size. InstantGroup features a Dual VAEs backbone with shared-weight twin networks to handle pairs of inputs and incorporates a Displacement Inversion Module (DIM) to maintain template unbiasedness and a Subject-Template Alignment Module (STAM) to improve template quality and registration accuracy. Experiments on 3D brain MRI scans from the OASIS and ADNI datasets reveal that InstantGroup dramatically reduces runtime, generating templates within seconds for various group sizes while maintaining superior performance compared to state-of-the-art baselines on quantitative metrics, including unbiasedness and registration accuracy.

**Index Terms**—Deep Generative Models, Template Generation, Groupwise Registration, Brain MRI images

## I. INTRODUCTION

**A**LIGNING anatomical structures into a common reference space is crucial for identifying and measuring structural differences and changes indicative of various conditions or diseases while minimizing individual differences [1], [2]. In medical image analysis, this alignment facilitates enhanced diagnosis and effective treatment planning by providing a standardized way to compare anatomical features, thus reducing the variability that can obscure meaningful differences [3], [4]. For instance, subtle changes in brain structure due to neurodegenerative diseases like Alzheimer’s can be more readily identified when all subjects are registered to a common template [5].

The procedure involving aligning a set of images into a common space is groupwise image registration (GIR), a fundamental task in computer vision, medical image analysis, and time-series signals [6]. Unlike pairwise registration that registers one image to another, GIR simultaneously considers multiple images, aiming to find transformations that best map each group image to the common template (an example is shown in Figure 1 with an explicit template). Moreover, GIR supports advanced statistical analysis and machine learning applications. Reducing inter-subject variability and increasing statistical significance makes it possible to detect more negligible effects and relationships in the data [7], leading to more reliable and generalizable predictive models for diagnostic and prognostic purposes [8].

However, the common group space is implicit and not readily available most of the time, which presents a significant

challenge as the choice of the template greatly influences registration accuracy and bias. Performing pairwise registration or selecting a subject from the target group as the template can introduce uncertainties and bias, resulting in a deviated deformed group losing initial mutual information [1], [6]. While some groupwise registration methods do not rely on the template and perform direct groupwise registration [9]–[11], constructing an explicit template image has distinct advantages. The template can serve as a group representative for subsequent analysis tasks and enable parallel pairwise registration, improving efficiency.

Classic template construction algorithms such as iterative optimization methods [6], [12], [13] suffer from high computational costs, especially for 3D volumetric data. Some works [14], [15] committed to utilizing hierarchical structures that divide large groups into smaller ones. These methods can deal with significant anatomical variants and improve processing efficiency, but they still face overall runtime and scalability limitations. Recent advances in learning-based approaches [16]–[18] offer promising solutions by leveraging neural networks to learn optimal transformations and generate high-quality templates efficiently, making GIR more practical for large-scale and real-time applications [19]–[21]. Existing learning-based methods can be categorized into two approaches. The first approach learns parameters for registration and constructs the template image during the training [19]–[21]. Despite their effectiveness, these methods can be regarded as neural-network-based optimization; the templates are optimized for each group of images, which is a significant limitation. Another research direction in learning-based GIR focuses on predicting the deformation fields directly [9], [22] bypassing the need for iterative optimization to achieve faster registration but often constrained to fixed group settings.

Given these challenges, there is a core need for efficient and scalable learning-based GIR methods that can handle varying group sizes without compromising performance. We propose utilizing the arithmetic property of latent vectors in Variational Autoencoders (VAEs) [23], [24] that supports space exploration, including interpolation and arithmetics on the latent vectors [25], [26], to instantly generate templates for MRI groups of arbitrary sizes. Hence, we reshape and decompose the groupwise template generation into three steps: acquiring the latent representation of each group subject, performing vector averaging, and reconstructing the template from the mean latent vector. This framework ensures stable and unbiased template generation with significantly reduced runtime. Based on it, we introduce a dual VAE backbone inspired by siamese networks [27]–[29] to deal with paired

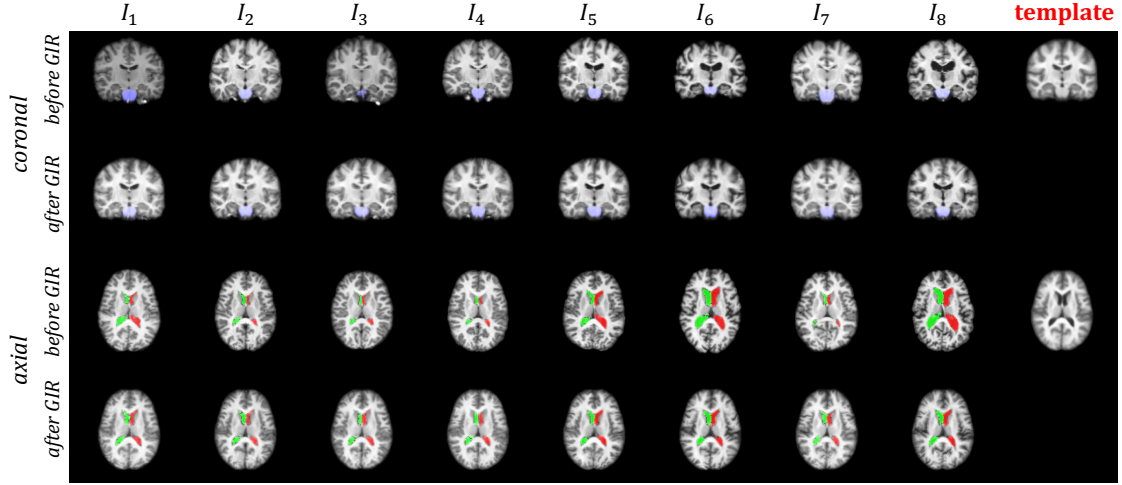


Fig. 1. Visualization of GIR on a sample group of brain MRIs with the template generated by InstantGroup. The figure shows coronal and axial views. The MRI scans pre- and post-GIR are displayed in rows 1, 3, and 2, 4, respectively. Deformed subjects Blue, green, and red masks denote the brain stem and left and right ventricles. The generated template is shown in the rightmost column in rows 1, 3.

inputs simultaneously using the VAEs with shared weights and get the template. By comparing the displacement fields from the paired symmetric paths to the template, we significantly improve groupwise registration performance. To summarize, our contribution can be concluded as follows:

- We are the first to utilize the latent representation of Dual VAEs with symmetric architectures to generate the template image efficiently for groupwise MRI image registration. The approach is scalable to problems of any scale with few additional costs;
- We propose the Displacement Inversion Module (DIM) to ensure the generated template is unbiased regarding the local deformation fields from all group subjects. We propose the Subject-Template Alignment Module (STAM) to compare images in the input space and improve the generated template;
- Experiments on two datasets of 3D brain MRI scans demonstrate that our method can achieve state-of-the-art performance in terms of unbiasedness and accuracy compared with baselines in a much shorter runtime from hours to seconds.

## II. RELATED WORK

### A. Pairwise Image Registration

Image registration generally involves aligning the moving image to the reference (fixed) image to minimize dissimilarity between them. Registration is challenging, especially for brains, due to anatomical complexity and significant inter- or intra-subject variations. Before deep learning-based image registration methods, traditional optimization-based methods involve the section of feature space, similarity measurement, the transformation type (local or global, rigid or non-rigid), and optimization strategy [30]. Rigid or affine transformations are mainly adopted in the registration of solid structures like bones or the pre-alignment before non-rigid registration [31], [32]. For most scenarios involving deformable subjects and

significant anatomical inconsistency, non-rigid transformation, mainly free-form deformation models, are used [33], [34].

Fueled by the thriving of deep learning technology, many works replace the erroneous iterative optimization with supervised/unsupervised learning or reinforcement learning models using neural networks [35]–[39]. VoxelMorph [40] utilizes the U-Net and the spatial transformer network to predict the deformation fields. Later, the diffeomorphic transformation was incorporated into the unsupervised framework [41] by predicting and integrating the velocity field to get the deformation field. To handle large deformation scenes, Mok and Chung [17] proposed a Laplacian pyramid network to solve the registration problem in a coarse-to-fine fashion. In many deep learning-based GIR methods, including the proposed method, diffeomorphic registration models are incorporated into the whole framework and generate the template.

### B. Learning-based groupwise image registration

Deep learning-based pairwise registration has significantly impacted the norm of GIR. Ahmad et al. [42] used deep neural networks to estimate the large initial deformations in the multi-level graph coarsening framework, improving the convergence speed. Dalca et al. [19] present a probabilistic model with diffeomorphic transforms for jointly template construction and registration, supporting conditional template generation given attributes. Dey et al. [20] added a discriminator to the framework for more authentic templates. Aladdin [21] introduced pairwise image losses with inputs in pairs and evaluated in image space via Atlas-as-a-bridge, improving overlap degree but lacking explicit template unbiasedness evaluation. These methods require optimization of the target group, limiting flexibility and increasing time consumption, especially with large datasets or varying group sizes.

Another approach develops models for different groups. He et al. [9] proposed an unsupervised learning scheme to predict deformation fields to warp subjects without explicit templates.

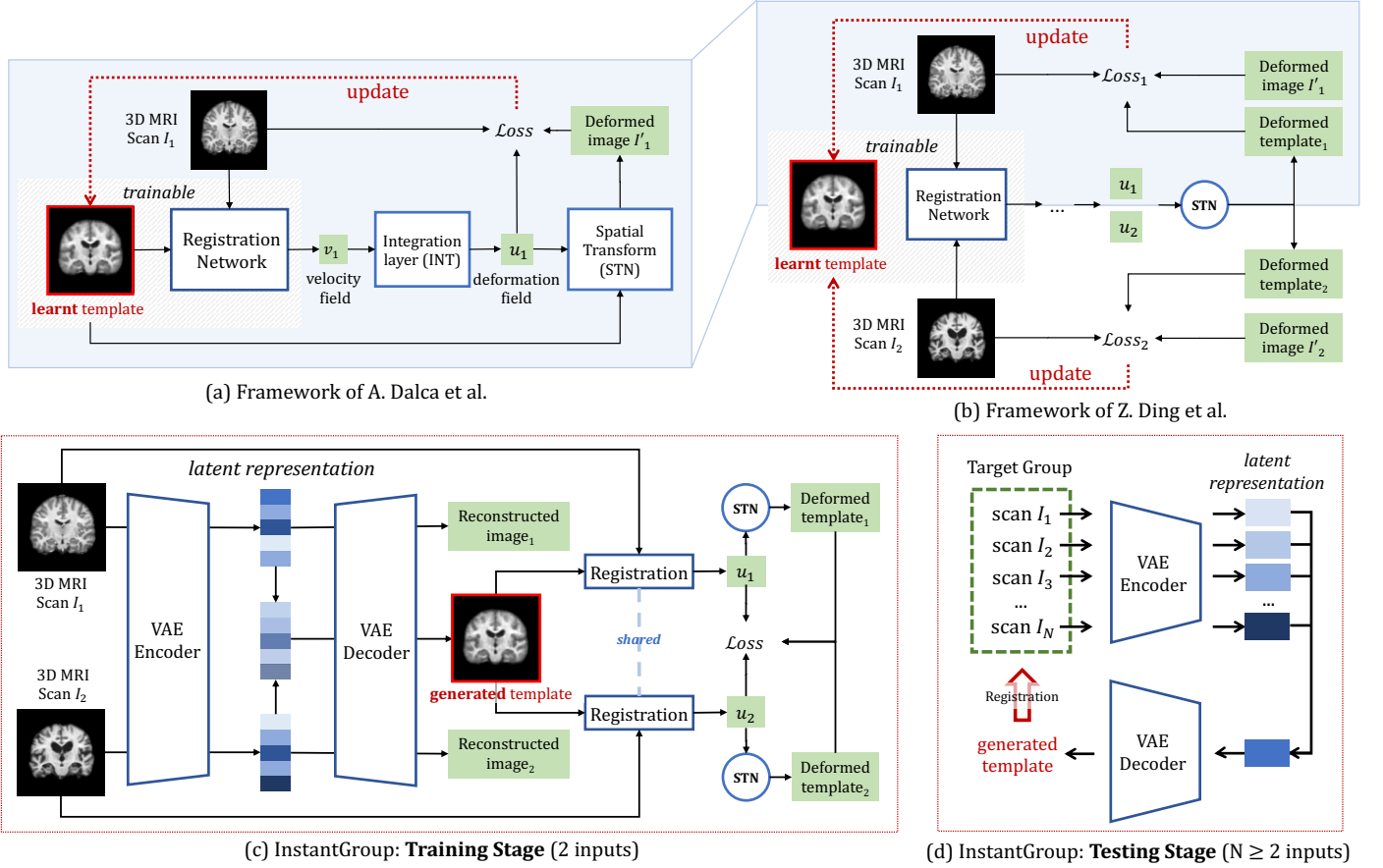


Fig. 2. Paradigm of baseline (a), (b) and the proposed InstantGroup (c), (d). (a) The baseline [19] for building deformable templates (unconditional version displayed). (b) The baseline [21], which can be regarded as a doubled version of (a) with two inputs, incorporates pairwise image similarity losses in both atlas and image space to improve accuracy. Both baselines update the template tensor with each test group subject during the training stage. In contrast, the proposed method (c) takes a dual VAE backbone to decode the template from aggregated latent representations of paired inputs. The structure predicts templates instead of updating the template during training like (a) or (b). (d) The testing stage of InstantGroup, different from its training stage, scales to any group size by encoding subjects and averaging their latent vectors to generate the template.

Semantic information is used [43] in a segmentation-assisted GAN to improve GIR performance. GroupMorph [22] learns diffeomorphic velocity field distribution with the variational GIR method. These methods have short runtime due to end-to-end learning but are restricted to fixed group sizes, where networks trained on a specific group size could not generalize well to groups of different sizes. In this paper, we present InstantGroup, a novel GIR framework that combines the efficiency of learning-based models with the scalability of optimization-based models. InstantGroup can be applied to any new group of any size without additional training or optimization.

### C. Deep generative models

GIR usually involves generating a center image representing the target group. In the past decade of research, various deep generative models which learn the data representation and synthesize realistic images have shown great potential in high-quality image generation. Generative Adversarial Nets (GAN) [44] is proposed to model the generation as an adversarial process where the generative model learns the data distribution and the discriminative model evaluates the authenticity of the

generated image. Later, conditional GANs [45] model the conditional distribution to generate specified samples given auxiliary conditions. CycleGANs [46] is another landmark for translating an image from one domain to another without the need for training data in pairs. Research on GANs and variants [47], [48] remains active today, and many are applied to medical modalities [49]–[54] including MRI and CT.

Although GANs are known for efficiency and high-quality results, they usually suffer from unstable training and limited sample diversity. On the other hand, Variational Autoencoders (VAEs) [23] learn the data likelihood distribution explicitly. VAEs are comprised of two components: the encoder that compresses data into a low-dimension latent space and the decoder that reconstructs data from the latent input. More recently, VQ-VAE [26] trains the autoencoder with discrete latent space and maintains a codebook of latent vectors, allowing it to adapt to natural modalities and learn complex data distributions. Other related works for medical image analysis [55]–[60] illustrate the superior performance of VAEs in representation learning. Autoencoders have demonstrated their ability to interpolate latent vectors in many studies [61], [62], suggesting that data can be semantically distributed in latent space [25]. While the

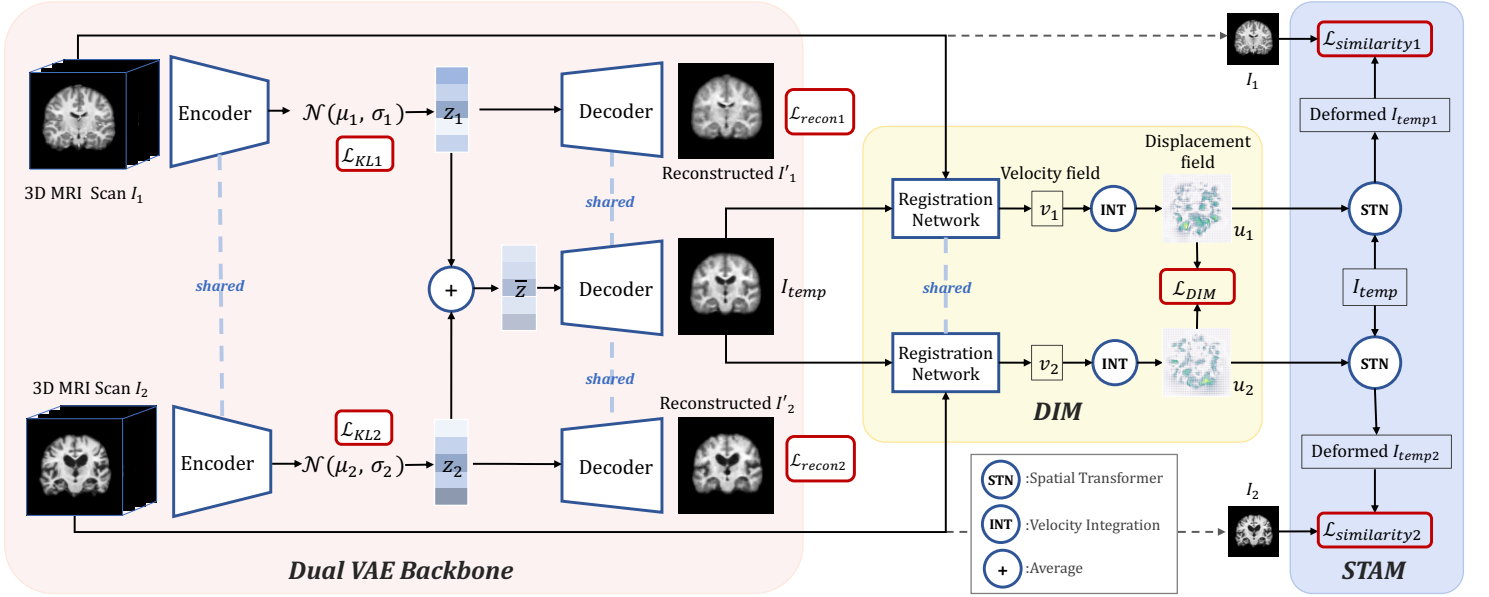


Fig. 3. Overview. The proposed method, InstantGroup, leverages a Dual VAE backbone for efficient and scalable high-quality template generation with DIM (Displacement Inversion Module) and STAM (Subject-Template Alignment Module). The Dual VAE backbone is a symmetric dual-path VAE architecture consisting of symmetrical upper and down parts with shared-weights encoder and decoder, allowing for the computation of the average latent vector  $\bar{z}$  and the generation of the template  $I_{temp}$  for each pair of input MRI scans. The Displacement Inversion Module (DIM) ensures unbiased template generation at the level of registration distance with a diffeomorphic registration network is applied to predict velocity fields  $v$ , integrated into deformation fields  $\phi$  to deform  $I_{temp}$ . The Subject-Template Alignment Module (STAM) improves template quality by measuring the similarity between the deformed template and each input scan.

existing VAE algorithms cannot meet the requirements of atlas construction of groupwise registration, we propose additional regularization on VAEs to encourage the interpolated outputs to be closer to brain MRI scans and correlate the latent interpolation with registration distances.

Besides GANs and VAEs, diffusion models [63]–[65] start to show success in creating images of quality even higher than GAN. Inspired by non-equilibrium thermodynamics, diffusion models define a Markov chain that gradually adds Gaussian noise to input and learns to reverse it for data construction, resulting in a relatively low sampling speed.

### III. METHODS

In this section, we will introduce the structure of the proposed **InstantGroup**, a scalable and efficient groupwise template generation method. We present a comparison in Figure 2 of previous learning-based methods (a, b) [21] and the proposed method (c, d) to highlight the novelty of InstantGroup. (a) and (b) both construct frameworks to update the parameters of the template by minimizing loss function, which requires training on the test group for an optimal template, while InstantGroup provides different procedures for training (c) and testing stage (d). In training stage (c), a pair of scans are fed to the encoder-decoder simultaneously, and the networks are updated by losses involving the inputs and a temporary template image. In testing stage (d), the number of inputs (the group size) is not fixed or limited; all group subjects will be encoded, and the template is then decoded from the average latent representation. The detailed architecture is displayed in Figure 3.

#### A. Dual VAE Backbone

The proposed method utilizes the widely used generative model named variational autoencoders (VAEs) [23], [24] to encode the brain MRI scans into latent representation and decode them back. The encoder, parameterized by  $\Phi$ , encodes input  $x$  into an approximated multivariate latent distribution  $q_{\Phi}(z|x)$ . The decoder, parameterized by  $\theta$ , reconstructs the image  $\hat{x} \sim p_{\theta}(x|z)$  from the sampled latent representation vector  $z \sim q_{\Phi}(z|x)$ . Both the encoder and decoder employ 3D convolutional neural networks. The optimization objective is to maximize the reconstruction likelihood between  $x$  and  $\hat{x}$  while minimizing the KL divergence between the learned posterior  $q_{\Phi}(z|x)$  and the assumed normal prior distribution  $p(z)$ . A scaling factor  $\beta$  [66] is applied to the KL term for more flexible latent space representation:

$$\mathcal{L}(x; \Phi, \theta) = E_{q_{\Phi}(z|x)}[\log p_{\theta}(x|z)] - \beta KL(q_{\Phi}(z|x) || p_{\theta}(z)), \quad (1)$$

As shown in Figure 3(d), we leverage the arithmetic on latent vectors of VAEs to generate the explicit common center for MRI groups of arbitrary size, which overcomes the fixed-size limitation of previous learning-based methods. Given the group of  $N$  MRI subjects  $I_1, I_2, \dots, I_N$  over space  $\Omega \subset \mathbb{R}^3$  in the testing stage, we first feed them separately (can be in parallel) into the encoder and obtain their latent vectors  $z_1, z_2, \dots, z_N$ . Second, compute the average vector  $\bar{z} = \frac{1}{N} \sum_{i=1}^N z_i$ , which is the centroid of the representatives. Finally, the decoder constructs the template from  $\bar{z}$  for GIR.

$$\mathcal{L}_{DVAE} = \lambda_{KL} \sum_{i=1}^N \mathcal{L}_{KL_i} + \lambda_{recon} \sum_{i=1}^N \mathcal{L}_{recon_i}, \quad (2)$$

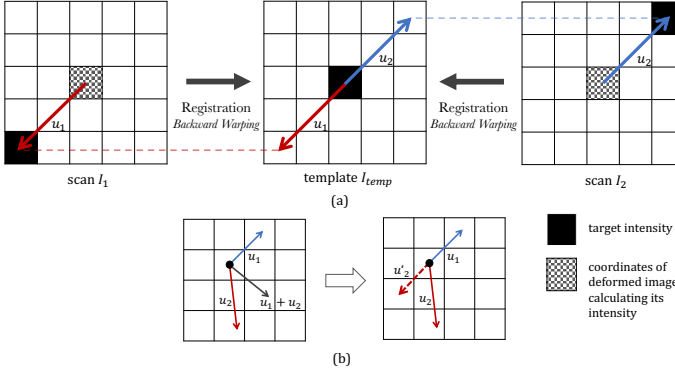


Fig. 4. (a) Backward warping that determines the original location of target voxels to calculate its intensity through interpolation. When registering  $I_1$  to  $I_{temp}$ , the displacement field indicates that the center pixel should be sampled from the value around the lower left corner, which is inverse of that of  $I_2$  to  $I_{temp}$ . (b) To minimize  $\|u_1 + u_2\|^2$ , the optimal vector is  $u'_2$  instead of  $u_2$ . Here, we use the notation  $u$  to denote the displacement vector at certain coordinates.

where  $\mathcal{L}_{recon_i}$  is the mean squared error between  $I_i$  and reconstructed  $I_i$ . Based on VAEs, we propose **Dual VAEs** that concurrently train two sets of VAEs that share the same networks and weights with a pair of input scans  $I_1$  and  $I_2$ . The encoder predicts the corresponding latent vector  $z_1, z_2$  of the inputs. Then the decoder reconstructs the input scans together with their representative template  $I_{temp}$  from  $\bar{z}$ . The Dual VAEs help narrow the leap from  $1 \rightarrow N$  to  $2 \rightarrow N$  when switching from the training to the testing stage.

The key advantage of the Dual VAEs backbone is handling dynamically any group size while learning to capture common features as well as the differences among the group subjects and the provided pairs of MRI scans as the minimal group to mimic the GIR scenarios in the testing stage.

### B. Displacement Inversion Module

The Dual VAEs backbone learns a latent distribution of the dataset, enabling interpolation in the latent space and compression of a group to the template. However, the image decoded from the average latent vector is not an anatomically meaningful template that can be smoothly morphed between group subjects [25]. A template must be not only semantically representative but also anatomically centered and unbiased. We introduce the Displacement Inversion Module (**DIM**) with an embedded stationary velocity field (SVF) registration network to ensure the generation of anatomically unbiased templates, through which we encourage the interpolated outputs to be closer to brain MRI scans and correlate the latent interpolation with registration distances.

For two inputs  $I_1$  and  $I_2$ , InstantGroup generates the template image  $I_{temp}$  from the average latent vector. We perform pairwise registration from  $I_1$  to  $I_{temp}$  and  $I_2$  to  $I_{temp}$  using SVF-based registration methods [4], [19], [41], [67], [68] that model the deformation field  $\phi$  by integrating the predicted stationary velocity field  $v$  over time  $t = [0, 1]$ . The ordinary differential equation is given as follows:

$$\frac{\partial \phi_v^t}{\partial t} = v \circ \phi_v^t, \quad (3)$$

where  $\phi^0$  is the identity map. The neural network  $Reg$  takes two input images as the moving  $I_m$  and fixed  $I_f$  and predicts the stationary velocity field  $v = Reg(I_m, I_f)$ . Using *scaling and squaring* [69]–[71], we can numerically calculate the integration  $\phi^1$  (or  $\phi$ ) that deforms  $I_m$  to  $I_f$ . Diffeomorphism has the property of invertibility. The inverse deformation field  $\phi^{-1}$  that deforms  $I_f$  to  $I_m$  can be computed by integrating the negative velocity field  $\phi_v^{-1} = \phi_{-v}$ . The differentiable spatial transform module  $STN$  computes each (sub)voxel linearly interpolated from neighboring voxels at the mapped location through the deformation field  $\phi$ . Let  $u$  be the displacement field representing the vector difference between the corresponding points in the moving and fixed images with  $\phi = Id + u$ , where  $Id$  is the identity transformation representing the original coordinates.

We adopt the displacement field to represent the geometric distance or variant between the template and input scans. As illustrated in Figure 4, backward image warping solves the coincide by assigning the original coordinates for the target pixels to refer to. We propose that the displacement vectors from all group subjects at each voxel of  $I_{temp}$  shall cancel out, resulting in the template voxel in equilibrium, which indicates its center position with even deformation distances to each subject, focusing on local discrepancies in the voxel level.

Combined with the Dual VAEs backbone, to enforce the two displacement fields from  $I_1$  and  $I_2$  to the template to be inverse, i.e., of the same magnitude in opposite directions, we propose in **DIM** the loss term of the squared L2 norm of sum of  $u_1$  and  $u_2$  to enforce an similar distance between  $I_{temp}$  and each input,

$$\mathcal{L}_{DIM} = \|u_1 + u_2\|^2. \quad (4)$$

### C. Subject-Template Alignment Module

The Dual VAEs backbone generates a pair of subjects and the corresponding template, constituting the minimal unit of a group. To leverage this feature for improving the quality and reliability of the generated template, we introduce the Subject-Template Alignment Module (**STAM**). This module ensures consistency by measuring the similarity between the deformed templates and their corresponding moving inputs.

The three potential comparison combinations are (1) similarity between the deformed template and each input; (2) similarity between the deformed input scan and the template; (3) similarity between the deformed scans (towards the template). Considering the nature of generated templates as a form of the average representative is its less clear appearance, comparing deformed scans in the template space as (2) or (3) may not be accurate enough during the registration process. In addition, denoting the energy functional of minimizing the mean squared error between the deformed template and the input scan as  $E$ , using Gâteaux Variation for the template  $I_{temp}$ , it can be derived [21]:

$$\delta E(I_{temp}; dI_{temp}) = 2 \left\langle \sum_{i=1}^N (I_{temp} - I_i \circ \phi_i) |D\phi_i|, dI_{temp} \right\rangle \stackrel{!}{=} 0, \quad \forall dI_{temp}, \quad (5)$$



with the optimal template  $I_{temp}^*$  being:

$$I_{temp}^* = \frac{\sum_{i=1}^N I_i \circ \phi_i |D\phi_i|}{\sum_{i=1}^N |D\phi_i|}, \quad (6)$$

where  $D$  denotes the Jacobian. The optimal template indicated constraints on the similarity between inputs, and the deformed template would push the template to a weighted average depending on the deformation fields. Therefore, we apply a constraint  $\mathcal{L}_{STAM}$  that measures the similarity between the deformed template  $I_{temp} \circ \phi_i$  and each scan in the input space:

$$\mathcal{L}_{STAM} = \sum_{i \in \{1,2\}} \mathcal{L}_{similarity}(I_{temp} \circ \phi_i, I_i), \quad (7)$$

where  $\phi_k$  represents the deformation field from  $I_{temp}$  to  $I_k$ , and  $\mathcal{L}_{sim}$  notes the dissimilarity measurement, which is the mean squared error.

#### D. Training and testing settings, and implementation

1) *Training stage*: The framework is trained with Dual VAEs as shown in Figure 3 and optimized by the overall loss function. In the training stage, two scans are fed into the networks and processed through dual symmetric paths via the share-weighted encoder, decoder, and registration module. The diffeomorphic registration neural network is pre-trained and frozen during the InstantGroup training. The framework is optimized by the overall objective loss function:

$$\mathcal{L}(I_1, I_2) = \mathcal{L}_{DVAE} + \lambda_{dim} \mathcal{L}_{DIM} + \lambda_{stam} \mathcal{L}_{STAM}. \quad (8)$$

2) *Testing stage*: The testing stage is displayed in Fig. 2 (d). Given a group of  $N$  MRI subjects, we encode them to latent vectors  $z_1, \dots, z_N$  and average  $\bar{z} = \frac{1}{N} \sum z_i$ . The decoder reconstructs the template image from  $\bar{z}$ . Therefore, **InstantGroup** can be applied to groups of different sizes.

3) *Implementation*: We implement the proposed InstantGroup using PyTorch [72]. The encoder is comprised of four 3D convolution modules with 128, 128, 128, and 256 filters. Each module contains a 3D convolution (kernel size=3, stride=2, padding=1) followed by LeakyReLU. The encoder outputs the mean  $\mu$  and log variance  $\log(\sigma)$  of a normal distribution; the reparameterization trick [23] is applied to sample vectors from the distribution. The latent representation  $z$  is of shape  $128 \times 6 \times 7 \times 6$ . The decoder employs four 3D transposed convolutions (kernel size=3, stride=2, padding=1) with 128, 128, 128, and 128 filters with LeakyReLU activation. The final convolution is activated by the sigmoid. After random searching, we obtain the optimal hyperparameters as  $\lambda_{recon} = 300$ ,  $\lambda_{KL} = 0.0002$ ,  $\lambda_{dim} = 7.5$ ,  $\lambda_{stam} = 100$ . The training time for OASIS and ADNI is approximately 21 hours (6 hours for 300 epochs VAE pretraining and 15 hours for 100k iterations InstantGroup training) and 62 hours (14 hours for 300 epochs VAE training and 48 hours for 300k iterations InstantGroup training) respectively. Parameters are optimized using Adam with an initial  $1e-4$  learning rate and decreased by a cosine annealing schedule ( $T = 4$ ). The diffeomorphic registration network is developed from the official implementation of VoxelMorph [73] with default hyperparameters and trained for 30k iterations.

## IV. EXPERIMENTS

### A. Datasets

1) *OASIS*: The Open Access Series of Imaging Studies (OASIS-1: Cross-sectional MRI Data in Young, Middle Aged, Nondemented and Demented Older Adults) [74] consists of T1-weighted MRI scans obtained from 416 subjects aged from 18 to 96 with 48 annotated segmentation labels. All volumes were preprocessed [75], including skull stripping, intensity normalization, affine registration to MNI brain space (Colin27), cropped and resampled to  $96 \times 112 \times 96$ . We utilize 30 anatomical structures as the segmentation ground truth for overlap evaluation. The dataset is divided into 305/40/80 as training, validation, and test sets.

2) *ADNI*: The Alzheimer’s Disease Neuroimaging Initiative (ADNI) [5] is a public database for research on Alzheimer’s disease (AD), like detecting and tracking diseases’ progression. We apply Sequence Adaptive Multimodal SEGmentation (SAMSEG) of FreeSurfer to perform automatic segmentation, followed by preprocessing similar to OASIS. The dataset is divided into 635/40/200 as training/validation/test sets.

### B. Baseline methods

We compare InstantGroup with three traditional baseline methods ABSORB [76], ANTs [77]. ABSORB [76] uses affinity propagation [78] for clustering and bundling subjects using diffeomorphic demons [79] as the registration method. ANTs [77] implemented in the ANTs software package [3], estimates the optimal templates and optimizes the geometric component iteratively. The number of iterations is 4, and the gradient is 0.2.

We also include two recent learning-based methods, DeformT [19], and Aladdin [21]. The framework of the two learning-based methods is also displayed in Figure 2 (a), (b). DeformT [19] is a learning framework for building deformable conditional templates for a different group of subjects. We pre-train the network for 800 epochs; for each test group, we train it for another 600 iterations. Aladdin [21] performs jointly atlas building and registration with pairwise image alignment. We pre-train the network for ten epochs; for each test group, we train it for 400 epochs.

### C. Evaluation metrics

1) *Unbiasedness*: To measure the unbiasedness degree of generated templates, we apply two metrics proposed in [4] that utilize the magnitude related to the deformation field (warping each group subject to the template) to evaluate this quantitatively: **Centrality** that computes the 2-norm of the mean displacement field and **AvgDisp**, which refers to the average displacement magnitude:

$$Centrality = \frac{1}{N} \left\| \sum_i^N u_i \right\|_2, AvgDisp = \frac{1}{N} \sum_i^N \|u_i\|_2. \quad (9)$$

For both metrics, lower values indicate higher unbiasedness.

TABLE I

TEST TIME TABLE (DEFAULT UNIT IS SECONDS IF NOT SPECIFIED). VALUES IN THE FORMAT OF "> $x$ " REFER TO A RUNTIME MUCH LARGER THAN  $x$ .

Group size	2	4	8	16	32	64	128
<b>InstantGroup</b>	<b>1.350</b>	<b>2.486</b>	<b>5.128</b>	<b>9.958</b>	<b>20.55</b>	<b>40.88</b>	<b>81.56</b>
ABSORB	14.74	55.99	225.4	505.7	1448	>3000	>3000
ANTs	64.79	118.9	163.7	322.9	697.8	1223	>3000
Aladdin	241.2	858.5	2335	106 min	>300 min	>300 min	>300 min
DeformT	34.14 min	78.31 min	130.6 min	208.4 min	360.1 min	>400 min	>400 min

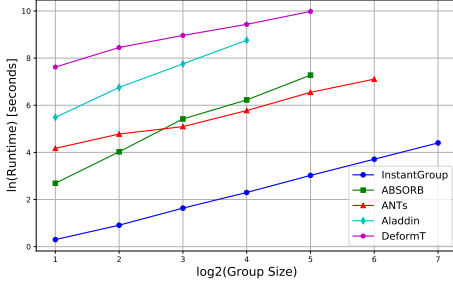


Fig. 5. Runtime (seconds in natural logarithm) comparison of the proposed method and baselines across different group sizes (in the log with base 2). Note that runtime in Table I without exact values is omitted.

2) *Dice score and Hausdorff distance*: In addition to Centrality and AvgDisp evaluating the unbiasedness of the generated templates, we also evaluate the registration accuracy with the template. We apply the widely used Dice Similarity Coefficient **DSC** to evaluate the template quality and group-wise registration performance, indicating the degree to which subjects warped to the same space. To eliminate the impact of potential template quality deviations, we compute the average anatomical label overlap between each warped group subject pair instead of that between subjects and templates. The formula is given as follows:

$$DSC = \frac{1}{N^2 N_s} \sum_{i,j} \sum_k \frac{2 \times |W_i^k \cap W_j^k|}{|W_i^k| + |W_j^k|}, \quad (10)$$

where  $N$  refers to the group size,  $N_s = 17$  refers to the number of labels,  $W_i^k$  is the pixel set of  $k_{th}$  region of  $i_{th}$  warped subject. Higher scores refer to better performance.

We also utilize the 95% percentile of the Hausdorff distance (**HD95**) to measure the distance between each pair of warped group subjects to reflect the robustness of the GIR method.

#### D. Runtime Analysis

We present the runtime of different group sizes ranging from 2 to 128 in Table I. The proposed method, InstantGroup, exhibits significant runtime improvement over traditional as well as other learning-based baselines across all tested group sizes.

For small groups like 4 or 8 subjects, InstantGroup generates the template in just seconds. As the group size increases, InstantGroup continues to scale efficiently. The runtime grows almost linearly with the group size, showcasing its scalability. For instance, InstantGroup can process a group of 128 subjects

in just around 81 seconds, while ABSORB and ANTs take dramatically longer, with ANTs requiring over 3100 seconds and DeformT exceeding 400 minutes to converge. Compared with traditional methods, InstantGroup can process 128 subjects in less time than ABSORB or ANTs takes to process just 8 subjects. As the group size increases, InstantGroup can be over 40 times faster than these baselines.

For the learning-based methods, the runtime is counter-intuitively longer. This inefficiency arises as Aladdin and DeformT involve training or fine-tuning the parameters to optimize the templates until convergence, which demands substantial runtime. When the group size increases to 128, Aladdin and DeformT take over 300 and 400 minutes to process such large groups, making InstantGroup over 200 times faster. InstantGroup presents a significant reduction in runtime compared to other methods, which often take several minutes to hours to achieve the same task. The linear scalability of InstantGroup is a direct result of its design. As the group size increases, the performance gap between InstantGroup and other methods becomes even more pronounced.

Figure 5 plots the logarithm runtime comparison. InstantGroup stands out as the most efficient method able to scale linearly with group size. Such significant runtime savings make InstantGroup highly suitable for practical applications in medical image analysis, where time efficiency is crucial.

#### E. Quantitative results

Table II presents a comprehensive quantitative comparison of InstantGroup with baseline methods on the two datasets, OASIS and ADNI. The results indicate that InstantGroup consistently outperforms the baselines in terms of Centrality, Average Displacement (AvgDisp), Dice Similarity Coefficient (DSC), and Hausdorff Distance (HD95).

#### V. PERFORMANCE ON UNBIASEDNESS

For Centrality and AvgDisp, which assess the degree of unbiasedness and geometric center alignment in terms of the deformation fields, InstantGroup demonstrates superior performance on both datasets. Specifically, InstantGroup achieves a Centrality value of 164 on OASIS and 182 on ADNI (29.7% and 48.6% improvement), significantly lower than all other methods. This indicates that the displacement fields from each group subject to the template are more in equilibrium, and templates generated by InstantGroup are more evenly centered within the group with minimal bias toward any particular subject. Additionally, the AvgDisp of InstantGroup on OASIS is 895.5, 2.3% higher than the best, and the AvgDisp

TABLE II

QUANTITATIVE RESULTS OF THE EXPERIMENTS ON OASIS AND ADNI USING THE FOUR METRICS.  $\uparrow$  DENOTES BETTER PERFORMANCE WITH HIGHER VALUES AND  $\downarrow$  DENOTES BETTER PERFORMANCE WITH LOWER VALUES. "INITIAL" REFERS TO SUBJECTS BEFORE UNDERGOING GIR. RESULTS IN BOLD INDICATE THE BEST PERFORMANCE FOR EACH METRIC (SIGNIFICANTLY BETTER THAN THE SECOND BEST WITH  $p < 0.05$  IN PAIRED T-TEST). P-VALUES ARE CALCULATED BY PAIRED T-TEST OF THE DSC VALUE BETWEEN THE PROPOSED INSTANTGROUP AND OTHER BASELINES. WE PRESENT THE HIGHER RESULT BETWEEN THE P-VALUE ON OASIS AND ADNI.

Methods	OASIS				ADNI				p-value
	Centrality $\downarrow$	AvgDisp $\downarrow$	DSC $\uparrow$	HD95 $\downarrow$	Centrality $\downarrow$	AvgDisp $\downarrow$	DSC $\uparrow$	HD95 $\downarrow$	
Initial	-	-	$60.12 \pm 1.45$	$2.308 \pm 0.09$	-	-	$62.96 \pm 2.56$	$2.144 \pm 0.18$	$< 10^{-4}$
ANTs	$239 \pm 10$	<b><math>873.7 \pm 37</math></b>	$73.55 \pm 0.44$	$1.478 \pm 0.04$	$348 \pm 19$	$936.8 \pm 28$	$74.95 \pm 3.09$	$1.282 \pm 0.18$	$< 10^{-4}$
ABSORB	$743 \pm 57$	$1102 \pm 88$	$73.50 \pm 0.55$	$1.450 \pm 0.04$	$870 \pm 76$	$1198 \pm 94$	$74.87 \pm 2.92$	$1.276 \pm 0.16$	$3 \times 10^{-4}$
DeformT	$353 \pm 36$	$943.4 \pm 35$	$74.02 \pm 0.35$	$1.427 \pm 0.03$	$359 \pm 51$	$946.1 \pm 37$	$74.98 \pm 3.45$	$1.280 \pm 0.17$	$1.9 \times 10^{-2}$
Aladdin	$585 \pm 26$	$1035 \pm 53$	$74.04 \pm 0.42$	$1.431 \pm 0.03$	$682 \pm 45$	$1099 \pm 39$	$74.25 \pm 2.76$	$1.297 \pm 0.14$	$2.6 \times 10^{-2}$
<b>InstantGroup</b>	<b><math>168 \pm 3.0</math></b>	$895.6 \pm 36$	<b><math>74.16 \pm 0.38</math></b>	<b><math>1.414 \pm 0.03</math></b>	<b><math>179 \pm 17</math></b>	<b><math>920.2 \pm 25</math></b>	<b><math>75.31 \pm 3.10</math></b>	<b><math>1.267 \pm 0.17</math></b>	-

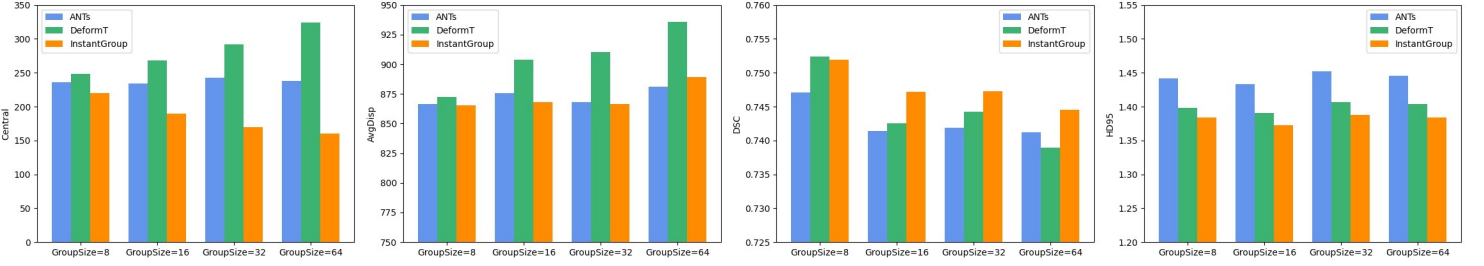


Fig. 6. Test groups of sizes 8, 16, 32, 64 compared to the two representative benchmarks ANTs and DeformT on all the four metrics Centrality, AvgDisp, DSC, and HD95. InstantGroup has comparable or superior robust performance across all group sizes.

of InstantGroup on ADNI is 920.2, 1.8% lower than the second best. The quantitative results validate the robustness of InstantGroup in generating templates that minimize the magnitude of displacements, leading to uniformity and consistency in the GIR process.

## VI. PERFORMANCE ON ANATOMICAL ALIGNMENT

InstantGroup achieves the highest DSC and the lowest HD95 on both datasets, indicating superior registration performance. Specifically, InstantGroup improves the DSC by approximately 0.19% over the second-best method (Aladdin) and reduces the HD95 by 0.91% compared to DeformT on the OASIS dataset. On the ADNI dataset, InstantGroup improves the DSC by 0.48% compared to DeformT and HD95 by 0.71% compared to ABSORB. All of the improvements are statistically significant, with p-values smaller than 0.05 in a paired t-test.

It is worth noting that the relatively modest improvements in DSC and HD95 are due to the fact that all methods use the same pairwise registration model to register group subjects to their templates. Since DSC and HD95 are more heavily influenced by the registration algorithm than the template generation process (which is the primary task of InstantGroup and baseline methods), the difference between InstantGroup and baselines can be minor. In addition, groupwise DSC tends to be lower compared to pairwise DSC since the subjects are registered to the medium (template) rather than being registered directly to each other. This characteristic inherently results in lower values and minor differences in DSC and HD95 among these methods in the GIR evaluation.

1) *Multiple group size performance analysis:* Figure 6 shows the scalability of InstantGroup and two representative benchmarks, ANTs and DeformT, across various group sizes (8, 16, 32, and 64). InstantGroup maintains remarkable robustness and consistently demonstrates superior or comparable performance across all group sizes with higher DSC values and lower HD95 values. More critically, InstantGroup achieves low Centrality and AvgDisp across all group sizes indicating the template is a consistent center reference for each group. The improvement in Centrality is larger as the group size doubles to 32 and 64 when ANTs and DeformT struggle with larger groups. The comparison underscores the advantages of InstantGroup in consistently generating unbiased templates with competitive registration accuracy.

2) *Training stage curve:* We present the performance curve of InstantGroup on the validation and test groups in Figure 8 during training. The figure indicates that InstantGroup converges effectively. The model exhibits significant improvement during the early stage, followed by meticulous optimization through further training and stabilizing at a high value. The Centrality oscillates during the early stage, which could be attributed to the notable enhancement in initial template quality and pairwise registration performance. The Centrality is then decreased steadily. By visualizing the performance curve throughout the training, we provide insights into the stable optimization of the proposed method.

### A. Interpolation analysis and qualitative results

Figure 7 demonstrates that InstantGroup can interpolate the latent vectors of input images smoothly and generate



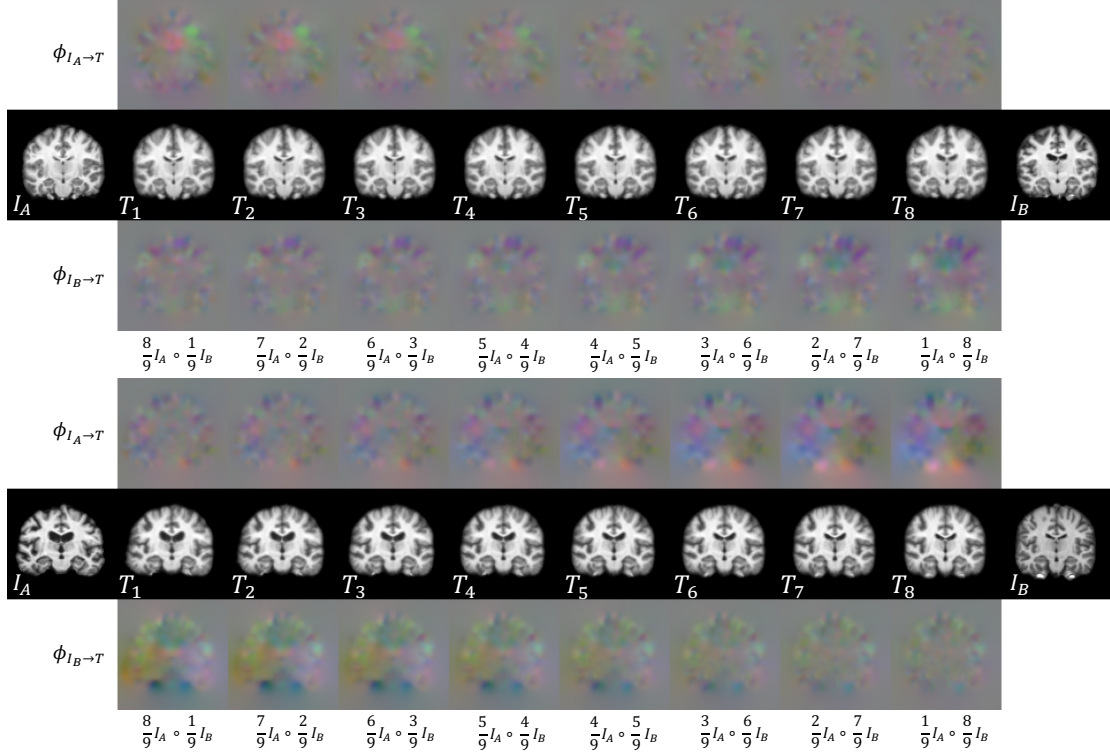


Fig. 7. Interpolation between two pairs of MRI scans  $I_A$  and  $I_B$ . The interpolated images  $T_k$  displayed in row 2 (and 5), column 2 to 9, are decoded from  $\frac{k}{9}z_A + \frac{9-k}{9}z_B$ , where  $z_A, z_B$  refers to the latent representation of the input  $I_A$  and  $I_B$ . Row 1 (and 4) and 3 (and 6) present displacement fields from  $I_A$  to  $T_k$  and from  $I_B$  to  $T_k$ . The displacement in x, y, and z dimensions is mapped to RGB channels.

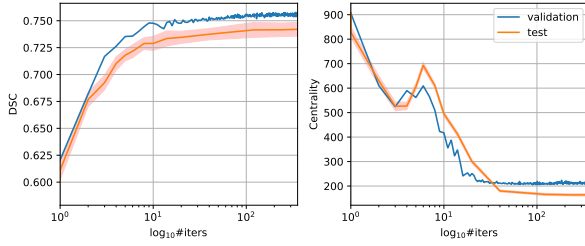


Fig. 8. The curve of GIR performance on the validation group and test groups during the training stage. The results of the test set are presented with the standard deviation band. #iters refers to  $10^3$  iterations.

semantically meaningful fusions. The interpolation process between a pair of MRI scans ( $I_A$  and  $I_B$ ) illustrates how the method preserves anatomical continuity and structural details while transitioning from one scan to another. The magnitude of displacement fields  $\phi_{I_A \rightarrow T}$ ,  $\phi_{I_B \rightarrow T}$  from one input to the interpolation images ( $T_1$  to  $T_8$ ) increases proportionally with the distance in the latent space as the interpolation progresses.

Evaluating template quality is challenging since segmenting the template itself may not be accurate since the template, being a form of the semantic average, often lacks clear anatomical structures [21]. Therefore, we can not measure the DSC or HD95 of deformed templates. Additionally, VAEs produce relatively blurred images due to its sampling. While the authenticity and details of InstantGroup templates are not comparable to real MR scans, they preserve overall anatomical

structures well, reducing high-frequency noise and enhancing robustness in subsequent registration tasks. Moreover, sharper templates do not necessarily guarantee better GIR results. The primary objective of GIR is to warp subjects to an unbiased center instead of the sharpness of the template. Overall, InstantGroup exhibits a remarkable ability to generate semantically unbiased and anatomically consistent templates effectively.

### B. Analysis of network design

1) *Ablation study on each component:* We conduct an ablation study on the validation group to investigate the impact of each module and loss term within InstantGroup, as shown in Table III. Method (a) refers to a naive baseline that iteratively generates the template by taking the average of all (deformed) group subjects. Method (b) refers to utilizing the latent arithmetics with Dual VAEs, which have templates with relatively low Dice Score and high bias as indicated by centrality and avgDisp values. As the DSC indicates, adding STAM (c) significantly improves registration accuracy. We can also observe a significant reduction in Centrality and AvgDisp when introducing DIM (d). The method (e) InstantGroup incorporates all proposed loss terms, yielding the highest Dice Score and lowest Centrality and AvgDisp values, indicating the successful integration of all components.

The architecture difference between InstantGroup and (a) can be summarized as that the former aggregates the group subjects on the level of latent space, while the latter simply on

TABLE III

ABLATION STUDY OF EACH COMPONENT OF INSTANTGROUP.(A) REFERS TO A NAIVE GIR METHOD THAT ITERATIVELY TAKES THE AVERAGE OF DEFORMED SUBJECTS. (B-D) REPRESENT COMBINATIONS OF EACH MODULE. (F-H) REFER TO ADDING AN EXTRA LOSS  $\mathcal{L}_{pair}$ .(E) IS THE PROPOSED METHOD INSTANTGROUP.(I) REPLACES  $\mathcal{L}_{DIM}$  BY THE OTHER VARIANT  $\mathcal{L}_{DIM-abl}$ .

Method	DualVAE	STAM	DIM	$\mathcal{L}_{pair}$	Centrality↓	AvgDisp↓	Dice ↑
a					853.4	1214	75.60
b	✓				338.8	871.3	75.05
c	✓	✓			299.3	874.3	75.47
d	✓		✓		198.7	809.4	75.51
<b>e (InstantGroup)</b>	✓	✓	✓		<b>184.8</b>	<b>805.7</b>	<b>75.85</b>
f	✓		✓	✓	215.2	834.9	75.49
g	✓	✓		✓	287.1	880.5	75.61
h	✓	✓	✓	✓	236.6	852.0	75.82
i	✓	✓	$\mathcal{L}_{DIM-abl}$		208.3	814.9	75.66

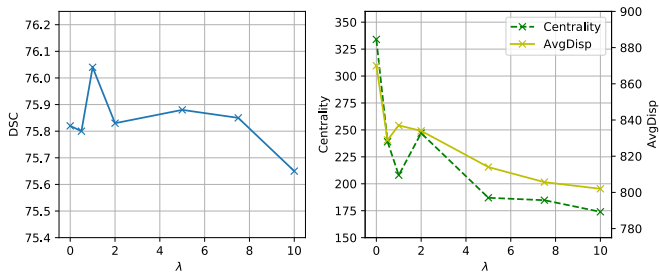


Fig. 9. Performance of InstantGroup on validation data with different hyperparameters  $\lambda_{dim}$  for  $\mathcal{L}_{DIM}$  for inverse displacement fields.

the pixel level. The difference results in huge gap in terms of the unbiasedness, proving InstantGroup’s superiority ensuring the generated template not only semantically representative but also anatomically unbiased, which is crucial for following groupwise analysis.

2) *Exploration on loss design:* We propose  $\mathcal{L}_{STAM}$  in InstantGroup to encourage the warped template to be close to the input. We explored adding the other similarity loss term that evaluates the pairwise alignment in the template space  $\mathcal{L}_{pair} = \mathcal{L}_{sim}(I_1 \circ \phi_1^{-1}, I_2 \circ \phi_2^{-1})$ . We add  $\mathcal{L}_{pair}$  to the framework and present the comparison as (f), (g), and (h). (h) achieves a high Dice Score but is less superior than (d) in Centrality and AvgDisp. As we compare (e) and (f) where the difference is to replace  $\mathcal{L}_{STAM}$  by  $\mathcal{L}_{pair}$ , the proposed InstantGroup exhibits the overall better performance.

Secondly, we replaced  $\mathcal{L}_{DIM}$  with its alternative (method e)  $\mathcal{L}_{DIM-abl} = ||u_1||_2^2 + ||u_2||_2^2$  that minimizes the total magnitude of the displacement fields instead of encouraging them to be inverse. The results demonstrate the advantage of the proposed method over the variant.

3) *Hyperparameters on unbiasedness regularization:* Figure 9 presents the Dice Score, Centrality, and AvgDisp for the validation group set with varying unbiasedness regularization hyperparameters  $\lambda_{dim}$ . The proposed loss term  $\mathcal{L}_{DIM}$  is designed to enforce the two displacement fields from the input images to the template to be inverse, thus encouraging the reconstructed middle template image to be at the center of the two inputs. When  $\lambda = 0$ , it represents the Dual VAEs without incorporating  $\mathcal{L}_{DIM}$ . The Dice Score demonstrates

an initial increase along the growth of  $\lambda_3$ , indicating that the regularization on unbiasedness can benefit the groupwise registration accuracy to a certain degree. When  $\lambda$  surpasses a threshold, the Dice Score starts to decline. The Centrality and AvgDisp steadily decrease with a higher regularization hyper-parameter on the unbiasedness term, which indicates better unbiasedness. Balancing the registration accuracy and unbiasedness leads to the selection of  $\lambda_{dim}$  within [5, 7.5].

## VII. CONCLUSION

In this paper, we propose InstantGroup, a scalable and efficient groupwise template generation framework, the first learning-based method capable of handling groups of any size without requiring extra training. We introduce a Dual VAEs backbone that processes pairs of inputs simultaneously using shared-weight networks with the Displacement Inversion Module (DIM) and Subject-Template Alignment Module (STAM). DIM ensures anatomically centered and unbiased template generation by enforcing inverse displacement fields from each input to the template. STAM improves the image quality and reliability by measuring the similarity between the deformed template and each input scan. Experimental results demonstrate that InstantGroup achieves superior unbiasedness and accuracy in template generation and drastically reduces computational time. Its flexibility and efficiency make it ideal for handling large-scale datasets. In conclusion, InstantGroup significantly advances GIR by providing a robust, efficient, and scalable solution for template generation.

## REFERENCES

- [1] V. Fonov, A. C. Evans, K. Botteron, C. R. Almli, R. C. McKinsty, D. L. Collins, B. D. C. Group *et al.*, “Unbiased average age-appropriate atlases for pediatric studies,” *Neuroimage*, vol. 54, no. 1, pp. 313–327, 2011.
- [2] M. Jenkinson, P. Bannister, M. Brady, and S. Smith, “Improved optimization for the robust and accurate linear registration and motion correction of brain images,” *Neuroimage*, vol. 17, no. 2, pp. 825–841, 2002.
- [3] B. B. Avants, C. L. Epstein, M. Grossman, and J. C. Gee, “Symmetric diffeomorphic image registration with cross-correlation: evaluating automated labeling of elderly and neurodegenerative brain,” *Medical image analysis*, vol. 12, no. 1, pp. 26–41, 2008.
- [4] J. Ashburner, “A fast diffeomorphic image registration algorithm,” *Neuroimage*, vol. 38, no. 1, pp. 95–113, 2007.

- [5] S. G. Mueller, M. W. Weiner, L. J. Thal, R. C. Petersen, C. R. Jack, W. Jagust, J. Q. Trojanowski, A. W. Toga, and L. Beckett, "Ways toward an early diagnosis in alzheimer's disease: the alzheimer's disease neuroimaging initiative (adni)," *Alzheimer's & Dementia*, vol. 1, no. 1, pp. 55–66, 2005.
- [6] S. Joshi, B. Davis, M. Jomier, and G. Gerig, "Unbiased diffeomorphic atlas construction for computational anatomy," *NeuroImage*, vol. 23, pp. S151–S160, 2004.
- [7] K. J. Friston, J. Ashburner, C. D. Frith, J.-B. Poline, J. D. Heather, and R. S. Frackowiak, "Spatial registration and normalization of images," *Human brain mapping*, vol. 3, no. 3, pp. 165–189, 1995.
- [8] V. Cheplygina, M. De Bruijne, and J. P. Pluim, "Not-so-supervised: a survey of semi-supervised, multi-instance, and transfer learning in medical image analysis," *Medical image analysis*, vol. 54, pp. 280–296, 2019.
- [9] Z. He and A. C. Chung, "Unsupervised end-to-end groupwise registration framework without generating templates," in *2020 IEEE International Conference on Image Processing (ICIP)*. IEEE, 2020, pp. 375–379.
- [10] R. Agier, S. Valette, R. Kéichichian, L. Fanton, and R. Prost, "Hubless keypoint-based 3d deformable groupwise registration," *Medical image analysis*, vol. 59, p. 101564, 2020.
- [11] S. Ying, G. Wu, Q. Wang, and D. Shen, "Hierarchical unbiased graph shrinkage (hugs): a novel groupwise registration for large data set," *NeuroImage*, vol. 84, pp. 626–638, 2014.
- [12] G. Wu, H. Jia, Q. Wang, and D. Shen, "Sharpmean: groupwise registration guided by sharp mean image and tree-based registration," *NeuroImage*, vol. 56, no. 4, pp. 1968–1981, 2011.
- [13] Q. Wang, D. Seghers, E. D'Agostino, F. Maes, D. Vandermeulen, P. Suetens, and A. Hammers, "Construction and validation of mean shape atlas templates for atlas-based brain image segmentation," in *Biennial International Conference on Information Processing in Medical Imaging*. Springer, 2005, pp. 689–700.
- [14] P. Dong, X. Cao, P.-T. Yap, and D. Shen, "Fast groupwise registration using multi-level and multi-resolution graph shrinkage," *Scientific reports*, vol. 9, no. 1, pp. 1–12, 2019.
- [15] M. R. Sabuncu, S. K. Balci, M. E. Shenton, and P. Golland, "Image-driven population analysis through mixture modeling," *IEEE transactions on medical imaging*, vol. 28, no. 9, pp. 1473–1487, 2009.
- [16] T. C. Mok and A. Chung, "Conditional deformable image registration with convolutional neural network," in *International Conference on Medical Image Computing and Computer-Assisted Intervention*. Springer, 2021, pp. 35–45.
- [17] —, "Large deformation diffeomorphic image registration with laplacian pyramid networks," in *International Conference on Medical Image Computing and Computer-Assisted Intervention*. Springer, 2020, pp. 211–221.
- [18] A. Hoopes, M. Hoffmann, B. Fischl, J. Guttag, and A. V. Dalca, "Hypermorph: amortized hyperparameter learning for image registration," in *International Conference on Information Processing in Medical Imaging*. Springer, 2021, pp. 3–17.
- [19] A. Dalca, M. Rakic, J. Guttag, and M. Sabuncu, "Learning conditional deformable templates with convolutional networks," *Advances in neural information processing systems*, vol. 32, 2019.
- [20] N. Dey, M. Ren, A. V. Dalca, and G. Gerig, "Generative adversarial registration for improved conditional deformable templates," in *Proceedings of the IEEE/CVF International Conference on Computer Vision*, 2021, pp. 3929–3941.
- [21] Z. Ding and M. Niethammer, "Aladdin: Joint atlas building and diffeomorphic registration learning with pairwise alignment," in *Proceedings of the IEEE/CVF Conference on Computer Vision and Pattern Recognition*, 2022, pp. 20 784–20 793.
- [22] T. F. van der Ouderaa, I. Išgum, W. B. Veldhuis, and B. D. d. Vos, "Deep group-wise variational diffeomorphic image registration," in *International Workshop on Thoracic Image Analysis*. Springer, 2020, pp. 155–164.
- [23] D. J. Rezende and M. Welling, "Auto-encoding variational bayes," *arXiv preprint arXiv:1312.6114*, 2013.
- [24] D. J. Rezende, S. Mohamed, and D. Wierstra, "Stochastic backpropagation and approximate inference in deep generative models," in *International conference on machine learning*. PMLR, 2014, pp. 1278–1286.
- [25] D. Berthelot, C. Raffel, A. Roy, and I. Goodfellow, "Understanding and improving interpolation in autoencoders via an adversarial regularizer," *arXiv preprint arXiv:1807.07543*, 2018.
- [26] A. Van Den Oord, O. Vinyals *et al.*, "Neural discrete representation learning," *Advances in neural information processing systems*, vol. 30, 2017.
- [27] J. Bromley, I. Guyon, Y. LeCun, E. Säckinger, and R. Shah, "Signature verification using a siamese time delay neural network," *Advances in neural information processing systems*, vol. 6, 1993.
- [28] G. Koch, R. Zemel, R. Salakhutdinov *et al.*, "Siamese neural networks for one-shot image recognition," in *ICML deep learning workshop*, vol. 2. Lille, 2015, p. 0.
- [29] R. R. Variator, M. Haloi, and G. Wang, "Gated siamese convolutional neural network architecture for human re-identification," in *European conference on computer vision*. Springer, 2016, pp. 791–808.
- [30] F. P. Oliveira and J. M. R. Tavares, "Medical image registration: a review," *Computer methods in biomechanics and biomedical engineering*, vol. 17, no. 2, pp. 73–93, 2014.
- [31] M. Andreetto, G. M. Cortelazzo, and L. Lucchese, "Frequency domain registration of computer tomography data," in *Proceedings. 2nd International Symposium on 3D Data Processing, Visualization and Transmission, 2004. 3DPVT 2004*. IEEE, 2004, pp. 550–557.
- [32] M. Auer, P. Regitnig, and G. A. Holzappel, "An automatic nonrigid registration for stained histological sections," *IEEE Transactions on Image Processing*, vol. 14, no. 4, pp. 475–486, 2005.
- [33] J. A. Schnabel, D. Rueckert, M. Quist, J. M. Blackall, A. D. Castellano-Smith, T. Hartkens, G. P. Penney, W. A. Hall, H. Liu, C. L. Truitt *et al.*, "A generic framework for non-rigid registration based on non-uniform multi-level free-form deformations," in *International Conference on Medical Image Computing and Computer-Assisted Intervention*. Springer, 2001, pp. 573–581.
- [34] S. Periaswamy and H. Farid, "Elastic registration in the presence of intensity variations," *IEEE transactions on medical imaging*, vol. 22, no. 7, pp. 865–874, 2003.
- [35] X. Chen, Y. Meng, Y. Zhao, R. Williams, S. R. Vallabhaneni, and Y. Zheng, "Learning unsupervised parameter-specific affine transformation for medical images registration," in *International Conference on Medical Image Computing and Computer-Assisted Intervention*. Springer, 2021, pp. 24–34.
- [36] T. C. Mok and A. Chung, "Affine medical image registration with coarse-to-fine vision transformer," in *Proceedings of the IEEE/CVF Conference on Computer Vision and Pattern Recognition*, 2022, pp. 20 835–20 844.
- [37] S. Zhao, T. Lau, J. Luo, I. Eric, C. Chang, and Y. Xu, "Unsupervised 3d end-to-end medical image registration with volume tweening network," *IEEE journal of biomedical and health informatics*, vol. 24, no. 5, pp. 1394–1404, 2019.
- [38] J. Hu, Z. Luo, X. Wang, S. Sun, Y. Yin, K. Cao, Q. Song, S. Lyu, and X. Wu, "End-to-end multimodal image registration via reinforcement learning," *Medical Image Analysis*, vol. 68, p. 101878, 2021.
- [39] R. Liao, S. Miao, P. de Tournemire, S. Grbic, A. Kamen, T. Mansi, and D. Comaniciu, "An artificial agent for robust image registration," in *Proceedings of the AAAI conference on artificial intelligence*, vol. 31, no. 1, 2017.
- [40] G. Balakrishnan, A. Zhao, M. R. Sabuncu, J. Guttag, and A. V. Dalca, "An unsupervised learning model for deformable medical image registration," in *Proceedings of the IEEE conference on computer vision and pattern recognition*, 2018, pp. 9252–9260.
- [41] A. V. Dalca, G. Balakrishnan, J. Guttag, and M. R. Sabuncu, "Unsupervised learning for fast probabilistic diffeomorphic registration," in *International Conference on Medical Image Computing and Computer-Assisted Intervention*. Springer, 2018, pp. 729–738.
- [42] S. Ahmad, J. Fan, P. Dong, X. Cao, P.-T. Yap, and D. Shen, "Deep learning deformation initialization for rapid groupwise registration of inhomogeneous image populations," *Frontiers in Neuroinformatics*, vol. 13, p. 34, 2019.
- [43] Z. He and A. Chung, "Learning-based template synthesis for groupwise image registration," in *International Workshop on Simulation and Synthesis in Medical Imaging*. Springer, 2021, pp. 55–66.
- [44] I. Goodfellow, J. Pouget-Abadie, M. Mirza, B. Xu, D. Warde-Farley, S. Ozair, A. Courville, and Y. Bengio, "Generative adversarial networks," *Communications of the ACM*, vol. 63, no. 11, pp. 139–144, 2020.
- [45] M. Mirza and S. Osindero, "Conditional generative adversarial nets," *arXiv preprint arXiv:1411.1784*, 2014.
- [46] J.-Y. Zhu, T. Park, P. Isola, and A. A. Efros, "Unpaired image-to-image translation using cycle-consistent adversarial networks," in *Proceedings of the IEEE international conference on computer vision*, 2017, pp. 2223–2232.
- [47] H. Zhang, T. Xu, H. Li, S. Zhang, X. Wang, X. Huang, and D. N. Metaxas, "Stackgan: Text to photo-realistic image synthesis with stacked

- generative adversarial networks,” in *Proceedings of the IEEE international conference on computer vision*, 2017, pp. 5907–5915.
- [48] T. Karras, T. Aila, S. Laine, and J. Lehtinen, “Progressive growing of gans for improved quality, stability, and variation,” *arXiv preprint arXiv:1710.10196*, 2017.
- [49] T. Karras, S. Laine, and T. Aila, “A style-based generator architecture for generative adversarial networks,” in *Proceedings of the IEEE/CVF conference on computer vision and pattern recognition*, 2019, pp. 4401–4410.
- [50] E. L. Denton, S. Chintala, R. Fergus *et al.*, “Deep generative image models using a laplacian pyramid of adversarial networks,” *Advances in neural information processing systems*, vol. 28, 2015.
- [51] X. Mao, Q. Li, H. Xie, R. Y. Lau, Z. Wang, and S. Paul Smolley, “Least squares generative adversarial networks,” in *Proceedings of the IEEE international conference on computer vision*, 2017, pp. 2794–2802.
- [52] S. Reed, Z. Akata, X. Yan, L. Logeswaran, B. Schiele, and H. Lee, “Generative adversarial text to image synthesis,” in *International conference on machine learning*. PMLR, 2016, pp. 1060–1069.
- [53] E. Kang, H. J. Koo, D. H. Yang, J. B. Seo, and J. C. Ye, “Cycle-consistent adversarial denoising network for multiphase coronary ct angiography,” *Medical physics*, vol. 46, no. 2, pp. 550–562, 2019.
- [54] K. Armanious, S. Gatidis, K. Nikolaou, B. Yang, and T. Kustner, “Retrospective correction of rigid and non-rigid mr motion artifacts using gans,” in *2019 IEEE 16th International Symposium on Biomedical Imaging (ISBI 2019)*. IEEE, 2019, pp. 1550–1554.
- [55] M. Shakeri, H. Lombaert, S. Tripathi, S. Kadoury, A. D. N. Initiative *et al.*, “Deep spectral-based shape features for alzheimer’s disease classification,” in *International Workshop on Spectral and Shape Analysis in Medical Imaging*. Springer, 2016, pp. 15–24.
- [56] C. Biffi, O. Oktay, G. Tarroni, W. Bai, A. D. Marvao, G. Doumou, M. Rajchl, R. Bedair, S. Prasad, S. Cook *et al.*, “Learning interpretable anatomical features through deep generative models: Application to cardiac remodeling,” in *International conference on medical image computing and computer-assisted intervention*. Springer, 2018, pp. 464–471.
- [57] M. Elbattah, C. Loughnane, J.-L. Guérin, R. Carette, F. Cilia, and G. Dequen, “Variational autoencoder for image-based augmentation of eye-tracking data,” *Journal of Imaging*, vol. 7, no. 5, p. 83, 2021.
- [58] V. Sandfort, K. Yan, P. M. Graff, P. J. Pickhardt, and R. M. Summers, “Use of variational autoencoders with unsupervised learning to detect incorrect organ segmentations at ct,” *Radiology: Artificial Intelligence*, vol. 3, no. 4, 2021.
- [59] R. Dorent, S. Joutard, M. Modat, S. Ourselin, and T. Vercauteren, “Hetero-modal variational encoder-decoder for joint modality completion and segmentation,” in *International Conference on Medical Image Computing and Computer-Assisted Intervention*. Springer, 2019, pp. 74–82.
- [60] D. Zimmerer, S. A. Kohl, J. Petersen, F. Isensee, and K. H. Maier-Hein, “Context-encoding variational autoencoder for unsupervised anomaly detection,” *arXiv preprint arXiv:1812.05941*, 2018.
- [61] A. Roberts, J. Engel, C. Raffel, C. Hawthorne, and D. Eck, “A hierarchical latent vector model for learning long-term structure in music,” in *International conference on machine learning*. PMLR, 2018, pp. 4364–4373.
- [62] D. Ha and D. Eck, “A neural representation of sketch drawings,” *arXiv preprint arXiv:1704.03477*, 2017.
- [63] J. Sohl-Dickstein, E. Weiss, N. Maheswaranathan, and S. Ganguli, “Deep unsupervised learning using nonequilibrium thermodynamics,” in *International Conference on Machine Learning*. PMLR, 2015, pp. 2256–2265.
- [64] J. Ho, A. Jain, and P. Abbeel, “Denoising diffusion probabilistic models,” *Advances in Neural Information Processing Systems*, vol. 33, pp. 6840–6851, 2020.
- [65] P. Dhariwal and A. Nichol, “Diffusion models beat gans on image synthesis,” *Advances in Neural Information Processing Systems*, vol. 34, pp. 8780–8794, 2021.
- [66] I. Higgins, L. Matthey, A. Pal, C. P. Burgess, X. Glorot, M. M. Botvinick, S. Mohamed, and A. Lerchner, “beta-vae: Learning basic visual concepts with a constrained variational framework,” *ICLR (Poster)*, vol. 3, 2017.
- [67] M. Hernandez, M. N. Bossa, and S. Olmos, “Registration of anatomical images using paths of diffeomorphisms parameterized with stationary vector field flows,” *International Journal of Computer Vision*, vol. 85, no. 3, pp. 291–306, 2009.
- [68] Z. Shen, X. Han, Z. Xu, and M. Niethammer, “Networks for joint affine and non-parametric image registration,” in *Proceedings of the IEEE/CVF Conference on Computer Vision and Pattern Recognition*, 2019, pp. 4224–4233.
- [69] V. Arsigny, O. Commowick, X. Pennec, and N. Ayache, “A log-euclidean framework for statistics on diffeomorphisms,” in *International Conference on Medical Image Computing and Computer-Assisted Intervention*. Springer, 2006, pp. 924–931.
- [70] J. Krebs, T. Mansi, B. Mailhé, N. Ayache, and H. Delingette, “Unsupervised probabilistic deformation modeling for robust diffeomorphic registration,” in *Deep Learning in Medical Image Analysis and Multimodal Learning for Clinical Decision Support*. Springer, 2018, pp. 101–109.
- [71] A. V. Dalca, G. Balakrishnan, J. Guttag, and M. R. Sabuncu, “Unsupervised learning of probabilistic diffeomorphic registration for images and surfaces,” *Medical image analysis*, vol. 57, pp. 226–236, 2019.
- [72] A. Paszke, S. Gross, S. Chintala, G. Chanan, E. Yang, Z. DeVito, Z. Lin, A. Desmaison, L. Antiga, and A. Lerer, “Automatic differentiation in pytorch,” 2017.
- [73] G. Balakrishnan, A. Zhao, M. R. Sabuncu, J. Guttag, and A. V. Dalca, “Voxelmorph: a learning framework for deformable medical image registration,” *IEEE transactions on medical imaging*, vol. 38, no. 8, pp. 1788–1800, 2019.
- [74] D. S. Marcus, T. H. Wang, J. Parker, J. G. Csernansky, J. C. Morris, and R. L. Buckner, “Open access series of imaging studies (oasis): cross-sectional mri data in young, middle aged, nondemented, and demented older adults,” *Journal of cognitive neuroscience*, vol. 19, no. 9, pp. 1498–1507, 2007.
- [75] Z. Yaniv, B. C. Lowekamp, H. J. Johnson, and R. Beare, “Simpleitk image-analysis notebooks: a collaborative environment for education and reproducible research,” *Journal of digital imaging*, vol. 31, no. 3, pp. 290–303, 2018.
- [76] H. Jia, G. Wu, Q. Wang, and D. Shen, “Absorb: Atlas building by self-organized registration and bundling,” *NeuroImage*, vol. 51, no. 3, pp. 1057–1070, 2010.
- [77] B. B. Avants, P. Yushkevich, J. Pluta, D. Minkoff, M. Korczykowski, J. Detre, and J. C. Gee, “The optimal template effect in hippocampus studies of diseased populations,” *Neuroimage*, vol. 49, no. 3, pp. 2457–2466, 2010.
- [78] B. J. Frey and D. Dueck, “Clustering by passing messages between data points,” *science*, vol. 315, no. 5814, pp. 972–976, 2007.
- [79] T. Vercauteren, X. Pennec, A. Perchant, and N. Ayache, “Diffeomorphic demons: Efficient non-parametric image registration,” *NeuroImage*, vol. 45, no. 1, pp. S61–S72, 2009.